JOURNAL OF GEOPHYSICAL RESEARCH, VOL. 100, NO. D10, PAGES 20,957–20,968, OCTOBER 20, 1995

Remote sensing of ClO and HCl over northern Scandinavia in winter 1992 with an airborne submillimeter radiometer

T. Wehr, S. Crewell,[1] K. Künzi, J. Langen,[2] H. Nett,[2] and J. Urban

Institute of Environmental Physics, University of Bremen, Bremen, Germany

P. Hartogh

Max-Planck-Institute for Aeronomy, Katlenburg-Lindau, Germany

Abstract. In February and March 1992 stratospheric ClO and HCl over northern Scandinavia were observed with the submillimeter-wave atmospheric sounder (SUMAS), as part of the European Arctic Stratospheric Ozone Experiment (EASOE). SUMAS is operated on board the German research aircraft Falcon and observes thermal emission lines in the frequency range 620–650 GHz. In this paper the instrument design and techniques to retrieve volume mixing ratios (VMR) from the measurement will be discussed. Results from the EASOE campaign will be presented including a detailed error analysis. A comparison of the retrieved profiles in the lower stratosphere indicates a strong decrease of ClO abundances from February to March, whereas no corresponding increase in HCl is observed.

Introduction

It is an accepted fact that stratospheric ozone is being destroyed effectively by chlorine of anthropogenic origin in a catalytic cycle [*Salawitch et al.*, 1993; *Solomon*, 1990]. Correlations of ozone depletion and high concentrations of ClO in Antarctica have been reported by *De Zafra et al.* [1989], *Solomon et al.* [1987], and *Anderson et al.* [1989]. Simultaneous global measurements of ClO and ozone have been presented by *Waters et al.* [1993]. ClO is considered a key substance in the catalytic cycle, and HCl is one of the major chlorine reservoir species. A model study of activation or deactivation of ClO_x for the EASOE winter is published by *Lutman et al.* [1994a, b]. The chlorine chemistry depends essentially on the conditions of the polar vortex, the dynamics of which are described for this winter by *Farman et al.* [1994].

A powerful tool to investigate the stratospheric chemistry and composition is remote sensing using submillimeter radiometry. Previously, ClO, HCl, O_3, and HO_2 were measured simultaneously by *Stachnik et al.* [1992] using a balloon-borne submillimeter heterodyne receiver. The airborne submillimeter-wave atmospheric sounder (SUMAS) measures thermal emission from rotational lines of HCl, ClO, and ozone. First results are reported by *Crewell et al.* [1994]. For the retrieval of vertical volume mixing ratio (VMR) profiles it is necessary to measure the pressure broadened lines with sufficiently high frequency resolution. The VMR profile retrieval is based on the theory of radiative transfer in the atmosphere, the knowledge of the spectroscopic data of the observed species, and other additional information, e.g., the temperature profile of the atmosphere. The error analysis takes into account all known errors and uncertainties and provides an estimate of the VMR profile errors.

Instrumental Design

SUMAS observes thermal emission lines in the frequency range of 620–650 GHz with an instantaneous bandwidth of 1.2 GHz. The system is a heterodyne receiver based on all solid-state technology. It is installed on board the research aircraft Falcon, which is operated by the German Air and Space Research Organization (DLR). The operational altitude is 10 to 12 km in order to avoid signal absorption through tropospheric water vapor.

The atmospheric emission enters the receiver front end at an elevation angle of 15°. It passes through the aircraft pressure window made of high-density polyethylene. The influence (emission and absorption) of the pressure window on the measured atmospheric signal must be known a priori because it is outside the calibration system. A calibration mirror switches the receiver

[1]Now at Physics Department, State University of New York, Stony Brook

[2]Now with European Space Research and Technology Centre, Noordwijk, Netherlands

Paper number 95JD01925.
0148-0227/95/95JD-01925$05.00

input, alternating between the atmospheric signal and two microwave absorbers, at liquid nitrogen temperature and room temperature, respectively.

Standing waves within the quasi-optics are suppressed by the path length modulator. It is verified in the laboratory that it reduces standing waves by a factor of 50. The proper function of the system accommodated in the aircraft was also verified by simulating strong feedback by inserting a reflective element into the signal path. During data retrieval, it could be verified that no additional correction of standing waves was necessary.

The unwanted sideband of the receiver is decoupled from the signal path by a quasi-optical single sideband filter. Single sideband filter and diplexer were realized by Martin-Puplett type interferometers. The sideband suppression is better than 20 dB [*Crewell*, 1993]. The local oscillator consists of an InP-Gunn oscillator operating in the range 106–107 GHz, followed by cascaded Schottky-diode multipliers (doubler plus tripler).

For the stronger HCl line an uncooled open structure Schottky mixer is used. The weak ClO line is detected with a waveguide Schottky mixer cooled to ~80 K.

The system noise temperature is typically 8700 K for the HCl receiver and 3900 K for the ClO receiver. For the inner 100 MHz this value is approximately 10 % better. Between flights, optimization and adjustment of the mixer, quasi-optics, and local oscillator as well as temperature changes during the flight can increase the system noise up to 15 %. For the VMR profile retrieval a conservative estimate of the system noise temperatures of 10,000 K (HCl) and 5000 K (ClO) is used.

The first intermediate frequency (IF) signal is located at 10 GHz (ClO) and 11.08 GHz (HCl). The IF signal is amplified by a low-noise high electron mobility transistor (HEMT) preamplifier stage, operating at ~80 K, followed by additional amplifiers, bandpass filters, and a second mixing stage. The back end of SUMAS contains three filter banks with resolutions 10 × 80 MHz, 8 × 40 MHz, and 10 × 8 MHz. The scientific data and housekeeping information from the aircraft are stored on 150 megabyte streamer tapes. Quick-look of the measured spectra is available on the instrument computer. Figure 1 shows a circuit diagram of SUMAS. For additional technical information the reader is referred to *Nett et al.* [1990, 1991a, b], *Crewell et al.* [1994] and, in particular, to *Crewell* [1993].

Retrieval Techniques

The quantity observed by the radiometer is the spectral power dw with the dimension [WHz^{-1}]. The spec-

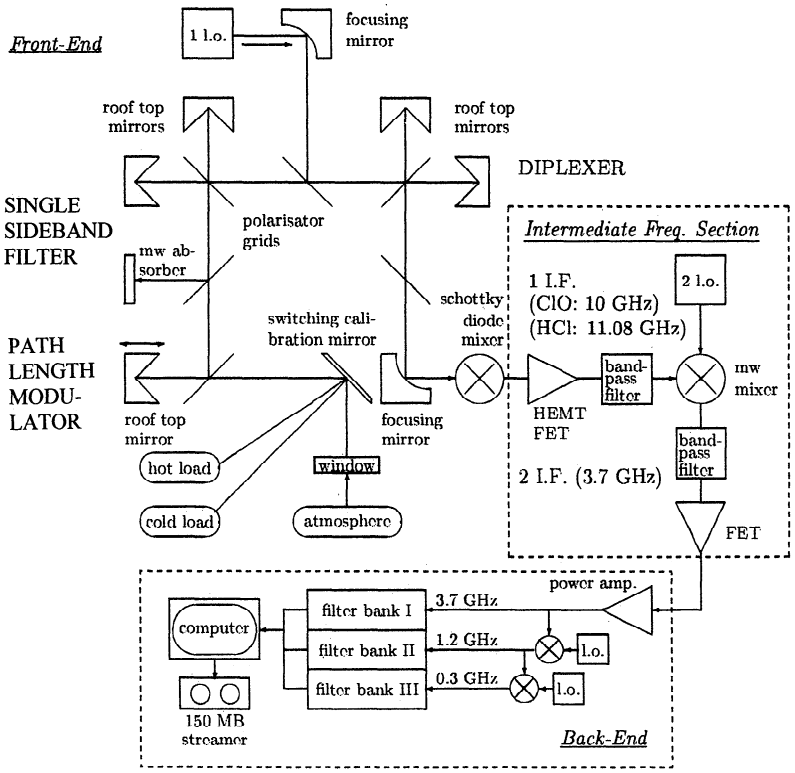

Figure 1. SUMAS circuit diagram. The atmospheric signal is calibrated by switching a mirror ("switching calibration mirror") successively between three positions: atmosphere, hot load (microwave absorber material at room temperature), and cold load (microwave absorber material in liquid nitrogen). For the HCl measurement the first mixer ("Schottky diode mixer") consists of an uncooled Schottky diode corner cube mixer, and for the ClO receiver a liquid nitrogen cooled Schottky diode wave guide mixer is used. The first intermediate frequency (1 I.F.) is located at 11.08 GHz for HCl and at 10 GHz for the ClO receiver.

tral power from a solid angle $d\Omega$ of the sky is a function of the brightness I_ν:

$$dw = I_\nu \cos\theta d\Omega dA \tag{1}$$

where θ is the angle between $d\Omega$ and zenith and dA is the infinitesimal area of surface. The spectra are presented in the more familiar unit of degrees Kelvin by dividing the spectral power by Boltzmann's constant. In the Rayleigh-Jeans limit this quantity is called brightness temperature.

The received emission from the atmosphere at the point of observation s_0 is given as the brightness I_ν, which is a function of the frequency ν. The radiative transfer equation can be written in the form

$$\begin{aligned} I_\nu(s_0) &= I_\nu(s_B)e^{-\tau(s_0,s_B)} \\ &+ \int_{s_0}^{s_B} \alpha_\nu(s)B_\nu(T(s))e^{-\tau(s_0,s)}ds \end{aligned} \tag{2}$$

This describes the received signal, where s_B is the maximum altitude of the atmosphere, i.e. the point above which the contribution of the atmospheric emission to the received signal can be neglected. Both the absorption coefficient α_ν and the source function $B_\nu(T(s))$ depend on the frequency ν and the atmospheric temperature $T(s)$. In the case of thermal emission the source function is equal to the Planck function assuming local thermodynamic equilibrium. The opacity is the total atmospheric absorption between s_0 and s_1:

$$\tau_\nu(s_0, s_1) = \int_{s_0}^{s_1} \alpha_\nu(s')ds' \tag{3}$$

The absorption coefficient α_ν is the sum of the absorption coefficients of all molecular lines and continuum contributing to the attenuation near ν. The background term $I_\nu(s_B)$ corresponds to the radiation due to the 2.7 K cosmic background temperature.

If the resonances are weak, the self-absorption can be neglected ($\tau_\nu \ll 1$). The absorption coefficient α_ν of one single transition as a function of frequency is given by *Waters* [1976]. The spectroscopic data of the relevant transitions are available from the Jet Propulsion Laboratory database [*Pickett et al.*, 1991]. The absorption coefficient α_ν is a linear function in VMR. The line shape is dominated by pressure broadening for stratospheric layers. Scattering is negligible in the stratosphere at submillimeter wavelengths.

Inverting equation (2) allows us to estimate the atmospheric VMR profile from a measured spectrum. Equation (2) is Fredholm's integral equation with no unique solution for its inverse. If (2) has to be solved for one species (e.g., ClO), the influence of all other atmospheric gases on the opacity must be known. In the discrete form the spectrum $\mathbf{y}$ is a vector calculated with the forward model F from the discrete VMR profile $\mathbf{x}$ and the vector of additional model parameters $\mathbf{b}$, e.g., temperature and pressure profile of the atmosphere and the pressure broadening coefficient of the observed emission line. The model parameter $\mathbf{b}$ enters the calculation of the weighting function matrix $\mathbf{K}$, which is in general, also dependent on $\mathbf{x}$. Equation (2) can be written in a matrix form (substituting the integral by a sum)

$$\mathbf{y} = F(\mathbf{x}, \mathbf{b}) = \mathbf{K}\mathbf{x} \qquad y_\nu = I_\nu(s_0) \tag{4}$$

The inverse model $I(\mathbf{y})$ provides the best estimate for the atmospheric parameter, i.e., the VMR profile of the interesting species. There are many retrieval techniques available to calculate $\mathbf{x}$ from the measurement $\mathbf{y}$ using (2) or (4). One straightforward method is the calculation of the generalized inverse of $\mathbf{K}$ using the singular value decomposition [*Ben-Israel*, 1974]. This technique is only useful if $\mathbf{K}$ is well conditioned, i.e., the condition number of $\mathbf{K}$ is small. The condition number indicates the maximum effect of perturbations in the spectrum to the solution $\hat{\mathbf{x}}$. One way to increase the condition of $\mathbf{K}$ is to reduce the number of unknown parameters, i.e., the number of atmospheric layers. Another stabilization method is to use the addition of a priori data. If an average state of the atmosphere and its uncertainty are known, this virtual measurement or a priori data can be combined with the real measurement, weighted by the error covariances. This leads to the optimal estimation method (OEM), described by *Rodgers* [1976]. If $\mathbf{y}$ is the measured spectrum and $\mathbf{S}_y$ its covariance matrix, the weighted average $\hat{\mathbf{x}}$ with the a priori VMR profile $\mathbf{x}_0$ and its covariance matrix $\mathbf{S}_x$ is given as

$$\hat{\mathbf{x}} = (\mathbf{S}_x^{-1} + \mathbf{K}^T\mathbf{S}_y^{-1}\mathbf{K})^{-1}(\mathbf{S}_x^{-1}\mathbf{x}_0 + \mathbf{K}^T\mathbf{S}_y^{-1}\mathbf{y}) \tag{5}$$

with the covariance matrix

$$\hat{\mathbf{S}} = (\mathbf{S}_x^{-1} + \mathbf{K}^T\mathbf{S}_y^{-1}\mathbf{K})^{-1} \tag{6}$$

where the exponents -1 and T denote the inverse and transpose, respectively, of a square nonsingular matrix, the circumflex symbol indicates that this value is estimated and not exactly known due to errors in $\mathbf{y}$ and the effect of the a priori information. For ClO retrieval, $\mathbf{K}$ is approximately independent of $\mathbf{x}$ because the ClO line is very weak. VMR profiles of ClO can be retrieved using (5) in a one-step algorithm. For HCl and O_3 retrieval, (5) is used iteratively. For every iteration, $\mathbf{K}$ is recalculated using the previous retrieved $\hat{\mathbf{x}}$, i.e., $\mathbf{K}^i = \mathbf{K}(F(\hat{\mathbf{x}}^{i-1}, \mathbf{b}))$. For HCl, two iterations have to be performed to achieve negligible changes in the VMR retrievals with further iterations.

In general, we describe the retrieval as the inverse function I of the forward model F or as the transfer function T of the real VMR profile:

$$\hat{\mathbf{x}} = I(F(\mathbf{x}, \mathbf{b}), \mathbf{b}, \mathbf{c}) = T(\mathbf{x}, \mathbf{b}, \mathbf{c}) \tag{7}$$

The additional vector $\mathbf{c}$ describes parameters which are only present in the retrieval model, e.g., the a priori VMR profile.

Error Analysis

A detailed general error characterization of retrieval techniques is given by *Rodgers* [1990] and has been

adapted in this paper. The total error of the retrieval I is given as an error covariance matrix $\mathbf{S}_T$ and is the sum of both statistical and model parameter errors. Every measurement $F(\mathbf{x}, \mathbf{b}) + \epsilon_y$ is the sum of the atmospheric signal depending on the real VMR $\mathbf{x}$, the real model parameters $\mathbf{b}$, and the statistical error ϵ_y. A forward calculation with a known $\mathbf{x}$ is $F(\mathbf{x}, \hat{\mathbf{b}})$ that uses not the exact model parameters $\mathbf{b}$ but their best estimate $\hat{\mathbf{b}}$. So the retrieval of a measurement is given as

$$\hat{\mathbf{x}} = I(F(\mathbf{x}, \mathbf{b}) + \epsilon_y, \hat{\mathbf{b}}, \mathbf{c}) \tag{8}$$

To linearize this equation, *Rodgers* [1990] defines the matrices $\mathbf{D}_\xi = \partial I / \partial \xi$ (derivatives of the retrieval model with respect to all parameters ξ) and $\mathbf{K}_\rho = \partial F / \partial \rho$ (derivatives of the forward model with respect to all parameters ρ). We linearize about the a priori $\mathbf{x}_0$ and obtain the total error of the retrieval

$$\hat{\mathbf{x}} - \mathbf{x} = \underbrace{(\mathbf{D}_y \mathbf{K}_x - \mathbf{I})(\mathbf{x} - \mathbf{x}_0)}_{N} + \underbrace{\mathbf{D}_y \mathbf{K}_b \epsilon_b}_{S} + \underbrace{\mathbf{D}_y \epsilon_y}_{M} \tag{9}$$

where $\mathbf{I}$ is the unity matrix. With these matrices the retrieval model (with a priori $\mathbf{x}_0$) can be written as

$$\hat{\mathbf{x}} = \mathbf{A}\mathbf{x} + (\mathbf{I} - \mathbf{A})\mathbf{x}_0 + \mathbf{D}_y \mathbf{K}_b \epsilon_b + \mathbf{D}_y \epsilon_y \tag{10}$$

The matrix $\mathbf{A} = \mathbf{D}_y \mathbf{K}_x$ is called the averaging kernel matrix and is in general not equal to the unity matrix. The retrieved profile is a combination of the smoothed real profile and the a priori data. The averaging kernel matrix therefore contains information about the vertical resolution of the observing system and the influence of a priori data. The null space error N depends on $\mathbf{D}_y \mathbf{K}_x$ and gives the variability in the real profile that cannot be seen by the observing system because of the smoothing effect. Uncertainties in the model parameters ϵ_b will lead to retrieval errors S. For the SUMAS retrievals the model parameters considered in the error analysis are the temperature and the pressure profiles and pressure broadening coefficients. The contribution of the measurement error ϵ_y to the retrieval error is M. All errors are given as covariance matrices, and their contribution to the retrieval error is calculated as described by *Rodgers* [1990].

Vertical Resolution

The assumption for the vertical resolution is that a VMR profile is vertically divided into different layers ("layer profile"), each of several kilometers thickness. Inside each layer, we assume a constant volume mixing ratio. The signal I_i received from a VMR layer profile is required to be the same as the signal from a profile with high vertical resolution. The signal from one layer with the thickness Δz is given after (4) as

$$I_i = \int_{\Delta z} K_i(z)\mathrm{VMR}(z)dz = \overline{\mathrm{VMR}} \int_{\Delta z} K_i(z)dz \tag{11}$$

That means that the signal from one layer is required to be proportional to the integrated weighting functions.

To find an appropriate low resolution (layer profile) of the retrieved VMR profile, the averaging kernel matrix of a representative ideal spectrum with a vertical resolution of 1 km is calculated to get an estimate of the smoothing effect of the measurement. Now the vertical resolution is reduced to get sufficiently small off-diagonal elements of the averaging kernel matrix, i.e., noncorrelated atmospheric layers and disappearing null space error. For comparability, we use the same resolution for all retrievals of one species and look at every averaging kernel matrix to see how significant the influence of the atmosphere is and how strong remaining correlations between the layers are.

Unfortunately, ClO and HCl cannot be evaluated with the same vertical resolution because the system noise temperature of the HCl receiver is higher than for the ClO receiver and the integration time for HCl measurements was much shorter. Therefore the stratosphere above 26 km contains only one value for HCl. The information content of lower stratospheric HCl is better than for ClO because both lines are contaminated by ozone line wings. This contamination could be eliminated much more accurately for HCl because O_3 is temporarily measured by the HCl receiver (see the following section on Spectra Preparation).

The use of a layer profile creates a representation error [*Rodgers*, 1990], i.e., the real atmosphere does not consist of the assumed layers, and the layer representation contains many fewer basic vectors of the VMR profile than the "continuous" VMR of the real atmosphere. Variations of the VMR within one layer cannot be seen in the layer profile because of the averaging procedure (11). The representation error is of about the same magnitude as the null space error of a VMR retrieval with high (1 km) vertical resolution.

Spectra Preparation

Before the retrieval technique (5) can be applied, the measured and calibrated spectra have to be corrected for the influence of the aircraft window. The window consists of a dielectric material with two parallel surfaces and therefore acts as a Fabry-Pérot interferometer, i.e., the measured atmospheric spectrum is offset by a modulated baseline, which has to be eliminated. The correction can be performed with the knowledge of the window parameters, i.e., its optical characteristics. The transmission can be estimated with a remaining uncertainty, leading to a residual error in the corrected spectrum, therefore contributing to the spectrum covariance matrix and eventually to the overall retrieval error. The window correction procedure for SUMAS has been very successfully modeled and described by *Crewell* [1993]. The remaining uncertainty of the window correction is small and fully correlated within the spectrum bandwidth; therefore the impact on the retrieval is almost negligible.

An additional contribution to the spectrum covariance is produced by the elimination of the ozone emission contaminating the ClO and HCl spectra. We use equation (5) for the retrieval of only one species,

i.e., we use it as for an atmosphere that contains no ozone. With the knowledge of the ozone VMR profile, we perform forward calculations of the appropriate ozone lines and subtract them from the ClO and HCl spectra. Therefore the ozone VMR profiles at the precise time and location of the observation are required. When observing HCl, the SUMAS can temporarily be switched into the other sideband to observe the 647.84-GHz ozone line. This allows an accurate estimate of the ozone VMR profile. For the ClO corrections, we used corresponding balloon-borne O_3 observations from the EASOE campaign. The uncertainties in our O_3 profiles contribute to the spectrum error covariance matrix.

The ClO signal absorption through O_3 is negligible, and the calculated ozone lines can be linearly subtracted. For HCl the absorption by O_3 is also weak, but not negligible. The amount of this effect can be calculated and corrected using a model HCl profile. The spectrum error due to this "nonlinear ozone correction" is a result of the model HCl profile error. Although we assume a large error in the model HCl profile, the amount of the error of the nonlinear ozone correction is small compared to the spectrum error covariance matrix due to measurement noise.

Continuum emission in the atmosphere, mainly due to water vapor, produces a roughly constant offset in the measured spectra with a variability of about 10 K. The amount of water vapor is still unknown because it is not measured simultaneously. Therefore, neglecting absorption effects, the absolute offset can be left as a free parameter to be retrieved. Due to the limited receiver bandwidth, the uncertainty in the spectral offset results in acquisition errors mainly for the far line wing contributions. This affects retrieval accuracy for lower stratospheric emission.

Data Evaluation

Example for ClO Measurement

For the illustration of the retrieval procedure in detail, the spectrum of the local flight of March 8, 1992, from Kiruna (north Sweden) to Finland is presented. A total of 433 single spectra along the flight route are averaged. Each single spectrum is an average over 4 s, thus yielding a total integration time of approximately 30 min. The frequency resolution at line center is 8 MHz, and the total bandwidth is 300 MHz. Figure 2 shows the measured spectrum and both the reproduced forward spectrum from the high-resolution retrieval (solid line) and the VMR layer profile (dotted line). The measured spectrum is offset, corrected with the retrieved offset parameter of the OEM layer profile retrieval. The retrieved spectrum offset parameter is anticorrelated to the ClO amount in the lower stratosphere. The reproduced spectrum of the high-resolution retrieval is stronger than the reproduced spectrum of the layer profile retrieval because the amount of ClO in the lower stratosphere is higher for the high-resolution retrieval. To plot the error bars of the measured spectrum in this figure would not be very meaningful because of the very strong off-diagonal elements of the covariance matrix, i.e., the diagonal elements are quite large but strongly correlated to the other channels. The covariance matrix mainly shows the structure of the uncertainty in the correction of the aircraft window emis-

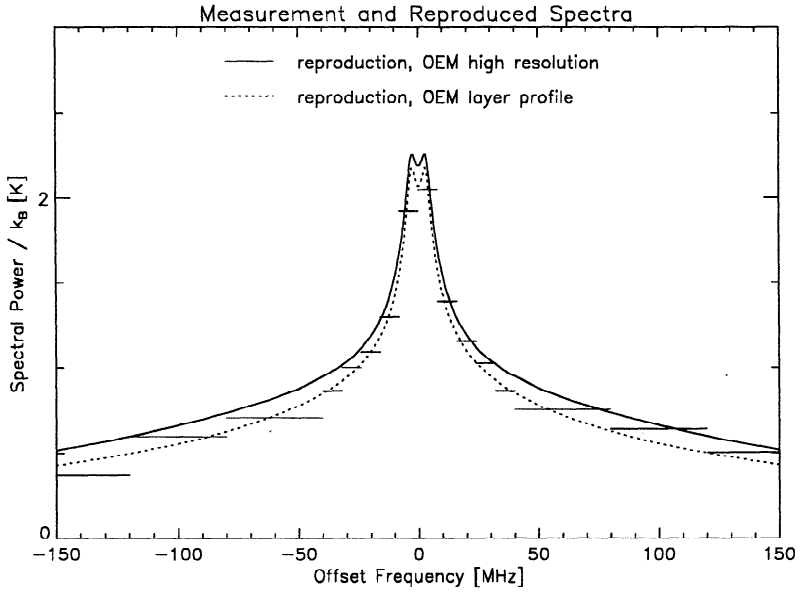

Figure 2. The measured spectrum of flight Kiruna-Finland, March 8, 1992, with reproduction of high-resolution OEM retrieval (solid line) and OEM layer profile (dotted line). The horizontal bars of the measured spectrum indicates the widths of the filter channels. The measured spectrum is offset-corrected with the retrieved offset parameter from the OEM layer profile retrieval. The reproduced spectra are not convoluted with the filter banks and therefore with high-frequency resolution.

sion, which leads to a remaining baseline uncertainty. Additional baseline uncertainties arise from the ozone signal elimination procedure, which is performed using balloon ozone sensor data with an optimal fit of time and location to the aircraft flight route but leaving uncertainties due to temporal and spatial differences. Spatial and temporary fluctuations in the ozone profiles obtained from different sensor data sets have been used to estimate uncertainties of the ozone profile along the flight route. Each element k_{ij} of the correlation coefficient matrix of the resulting error covariance matrix is calculated from the error covariance matrix elements c_{mn} with $k_{ij} = c_{ij}/\sqrt{c_{ii}c_{jj}}$. While large uncorrelated errors at the filter channels would lead to large uncertainties in the retrievals, the strong correlations (or anticorrelations) between the channels restrict the solution. The correlation coefficient matrix of the measured spectrum is presented in Figure 3.

This matrix indicates that the spectral power values at low frequencies are anticorrelated to the values at high frequencies. This results from baseline corrections, mainly from the correction of the influence of the aircraft pressure window. The remaining uncertainty of the window correction is of the same type as the modulated baseline from the Fabry-Pérot interferometer.

The retrieval of the measured spectrum with its covariance matrix is performed with the OEM using an a priori VMR profile with a diagonal covariance matrix and an uncertainty of σ=1 ppb for every 1-km altitude step. The retrieved VMR has been calculated both in 1-km steps and as a layer profile. The subdivision of the atmosphere into layers of constant VMR has been determined using typical measurement conditions to achieve an averaging kernel matrix approximately equal to the unity matrix. Figure 4 shows the results of the retrievals. Both the retrievals with high vertical resolution (1-km steps) and the low vertical resolution (layer profile) are presented. The $\pm 1\sigma$ errors of the layer profile are given as error bars. The $\pm 1\sigma$ error ranges of the high-resolution profile are plotted as dashed or dotted lines. The high-resolution retrieval yields a higher ClO amount in the lower stratosphere and a smaller spectrum offset in the measurement than the layer profile retrievals. The error analysis separates statistical and model parameter errors. For the inversion with 1-km resolution the statistical error is separated into the measurement error and the null space error. The diagonal elements of the null space error are of about the same magnitude as the a priori covariance diagonal elements, i.e., rapid vertical changes cannot be seen by the system because they are smoothed by the averaging kernels. The measurement error shows the uncertainties of the 1-km profile due to measurement errors. This error is relatively small, although the spectrum covariance matrix contains large values, but the mentioned strong correlations of the filter channels restrict the retrieval and reduce the measurement error in the retrieved VMR profile. The statistical error (= measurement error + null space error) of the layer profile is of about the same magnitude as the measurement error of the high vertical resolution profile in the upper layers, but is larger at lower altitudes. This behavior can be expected, since a constant offset had to be left as a free parameter for the retrieval procedure, i.e., the information of the lower layer remains only in the line shape but not in the absolute value of the measured line wings. This means, in terms of the averaging kernel matrix, that the kernel of the lowest layer disappears. This becomes clear when inspecting Figure 5 of the averag-

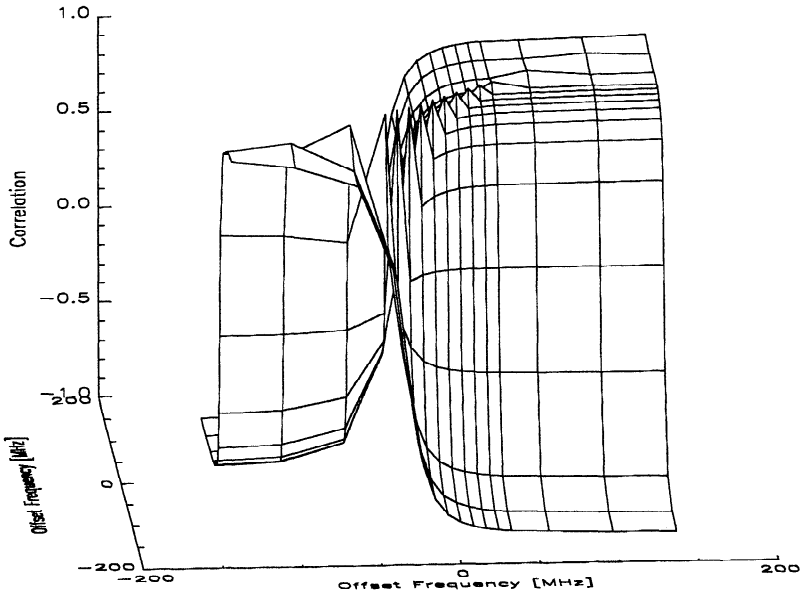

Figure 3. The correlation coefficient matrix of the spectrum covariance (March 8, 1992, flight VIII) shows strong correlations or anticorrelations of the filter channels.

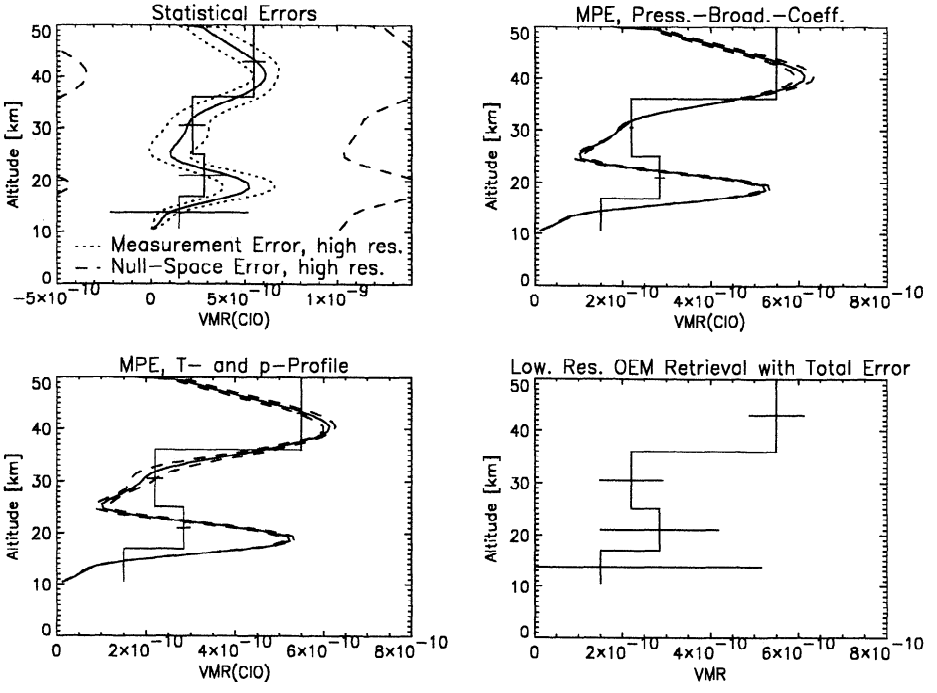

Figure 4. The retrieved profile (March 8, 1992, flight VIII) with high vertical resolution of 1 km and as a layer profile. The different error bars are the square roots of the corresponding covariance matrix diagonal elements, i.e., 1 σ error bars without taking the correlation into account. (Upper left) Statistical errors (measurement error and null space error). (Upper right and lower left) Errors due to uncertainties in the pressure broadening coefficient and in the temperature and pressure profile, respectively, i.e., errors due to model parameter errors (MPE). (Lower right) The total error bars.

ing kernel matrix. The lower layer data are dominated by the a priori information, while at higher altitudes the measurement data prevail. For all other EASOE retrievals, only the layers with a dominant influence of the measurement are presented.

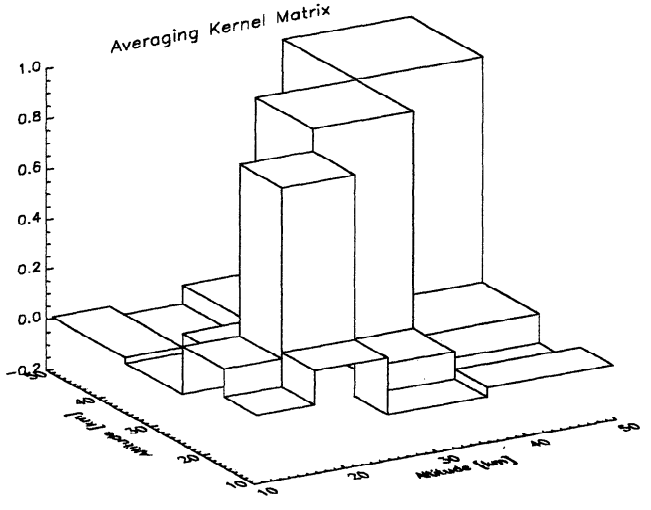

Figure 5. The averaging kernel matrix (March 8, 1992, flight VIII) shows that the measured spectrum has no influence on the lowest layer, a dominant influence of the 17–25 km layer, and full influence of the upper layers. The diagonal values are 0.06, 0.86, 0.95, 0.95. The off-diagonal elements are small, i.e., the correlations of the layers are weak.

The uncertainties of the model parameter **b** are divided into the errors due to errors in the pressure broadening coefficient and in the temperature and pressure profiles used for the retrievals. For the temperature profile a 10 K uncertainty at each height level and a 10% uncertainty for the surface pressure are assumed. This results in the retrieval errors presented in Figure 4 (lower left). For our retrievals these errors are small, but their covariance matrices contain large values for the off-diagonal elements. Even the impact of the uncertainty in the pressure broadening coefficient on the retrieval, presented in Figure 4 (upper left), is small. We use the measured pressure broadening coefficient of ClO at 649 GHz, published by *Oh and Cohen* [1994], with an error estimate of 3%. The uncertainty in the pressure broadening coefficient of HCl is larger. We use a theoretical calculation for the 625-GHz HCl line with an error estimate of 10% (Buffa, private communication, 1992). This calculation takes only self-broadening and N_2 collisions into account, but no broadening by O_2. Therefore we perform the error analysis with a coefficient uncertainty of 20%.

The sum of all single error covariance matrices (statistical errors and model parameter errors) is the total error covariance matrix, with the corresponding correlation coefficient matrix, shown in Figure 6. The square roots of the diagonal elements of the total error covariance matrix are plotted as the total $\pm 1\sigma$ errors of the retrievals (Figure 4, lower right). The correlation coef-

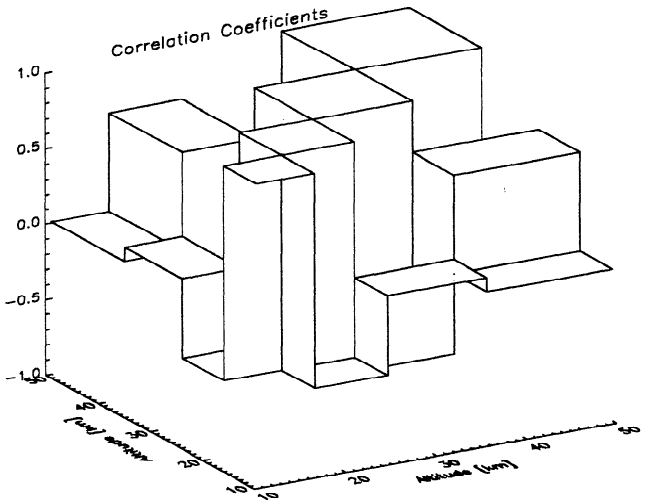

Figure 6. The correlation coefficients matrix (March 8, 1992, flight VIII) of the total error shows strong correlations and anticorrelations between the errors of the boxes.

ficient matrix (Figure 6) shows the strong correlations (or anticorrelations) of the layers, i.e., a variation of the VMR in one layer leads to an opposite VMR shift in the neighboring layers.

The calculation of a synthetic spectrum from each of these retrievals ("reproduction") shows a good fit to the measured data (Figure 2). The calculated offset values differ by 0.1 K. This difference is clearly inside the error range of the retrieved offset parameters, which is σ=0.47 K for the high-resolution retrieval and σ=0.42 K for the layer profile retrieval. This uncertainty corresponds to the large statistical errors in the lower stratospheric layers (Figure 4, upper left).

Results of EASOE Data Analysis

A preliminary analysis of some data are already published by *Crewell et al.* [1994]. This analysis did not perform a VMR profile retrieval but compared the integrated measured spectral power to the corresponding value of a synthetically calculated spectrum from a VMR model. The integrated spectral power was assumed to be proportional to the column density of the corresponding trace gas. With the VMR profile retrieval and analysis of systematic and statistical errors presented in this publication, the conclusions of *Crewell et al.* [1994] concerning ClO are basically consolidated. By analysis of some HCl data in the previous paper, it was stated that a significant increase in HCl from February to March was observed. With an analysis of the complete HCl data set and the VMR retrieval procedure including analysis of statistical and systematical errors, this statement has to be modified. The reason is the basically improved correction of the spectrum offset (continuum emission) with simultaneous VMR profile retrieval (see section above on spectra preparation). Additionally, in the preliminary analysis the VMR profile shape [World Meteorological Organization, 1985], used for the compared synthetic spectrum, contains no HCl below 30 km. Even the impact of the ozone emission line at 625.37 GHz on the HCl line has now been very accurately considered by retrieving the SUMAS ozone measurements of the 647.84-GHz ozone line.

The layer profile is preferred for EASOE data analysis in this paper rather than a high-resolution profile of 1-km steps because it yields approximately independent layers and avoids short-scale profile structures which are not necessarily real but rather artefacts due to error amplification by the retrieval technique, as shown by *Wehr* [1993].

The local flights from Kiruna and the transfer flights from Stockholm to Kiruna are presented here. The routes of the local flights are shown in Figure 7 and Table 1. Estimated VMR layer values are presented only if their corresponding averaging kernel matrix element is $\geq$0.6, i.e., the influence of the measurement is at least 60%. The error bars are the square roots of the corresponding diagonal elements of the total error covariance matrices. These matrices contain nonzero off-diagonal elements, i.e., the errors are correlated or anticorrelated.

The results of VMR retrievals are presented in Figures 8 and 9. Figure 8 shows the structure of the layer profiles. The error bars are the square roots of the diagonal elements of the total error covariance matrix of the retrieval, taking all known errors into account (see previous section, example for ClO measurement). The retrieved profiles of February and March are separately plotted for each observed region. The four upper plots show the ClO profiles, and the two lower plots the HCl data. Solid and dashed lines are February data, dotted lines are March data. The same data are presented in Figure 9 as a time series together with potential vorticity (PV at the 550 K level) values along the corresponding flight routes.

Analysis of European Centre for Medium-Range Weather Forecasts (ECMWF) data [*Braathen et al.*, 1992] shows that most flights were performed inside the polar vortex, here defined by the value 10^{-4} Km^2/kgs

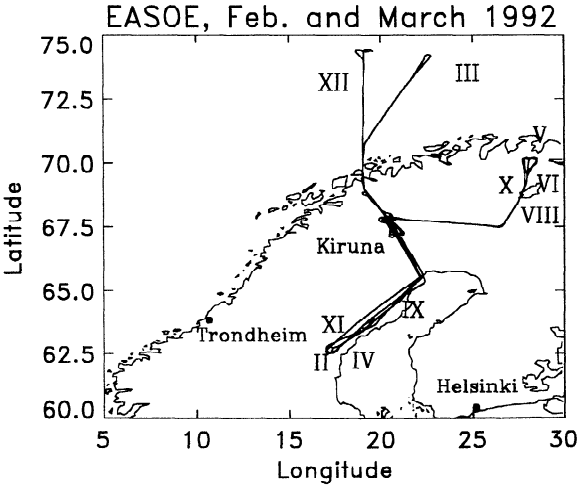

Figure 7. Local flight routes of SUMAS.

Table 1. Flight Routes of SUMAS, Measured Molecules, and Position in Terms of Potential Vorticity at 550 K Level

Flight	Date	Day	Route	Molecule	PV (550 K), 10^{-6}Km^2/kgs
I	Feb. 5	36	Stockholm – Kiruna	ClO	120–132
II	Feb. 6	37	Kiruna – South	ClO	120–132
III	Feb. 7	38	Kiruna – North	ClO	120–132
IV	Feb. 9	40	Kiruna – South	HCl, O_3	102–114
V	Feb. 10	41	Kiruna – Finland	HCl, O_3	108–120
VI	Feb. 12	43	Kiruna – Finland	ClO	114–126
VII[a]	March 7	67	Stockholm – Kiruna	ClO	66–126
VIII[b]	March 8	68	Kiruna – Finland	ClO	90–126
IX[b]	March 9	69	Kiruna – South	ClO	90–126
X	March 10	70	Kiruna – Finland	HCl, O_3	102–114
XI[b]	March 10	70	Kiruna – South	HCl, O_3	90–102
XII	March 12	72	Kiruna – North	ClO	114–126

[a] Flight across the vortex border.
[b] Flight close to the vortex border.

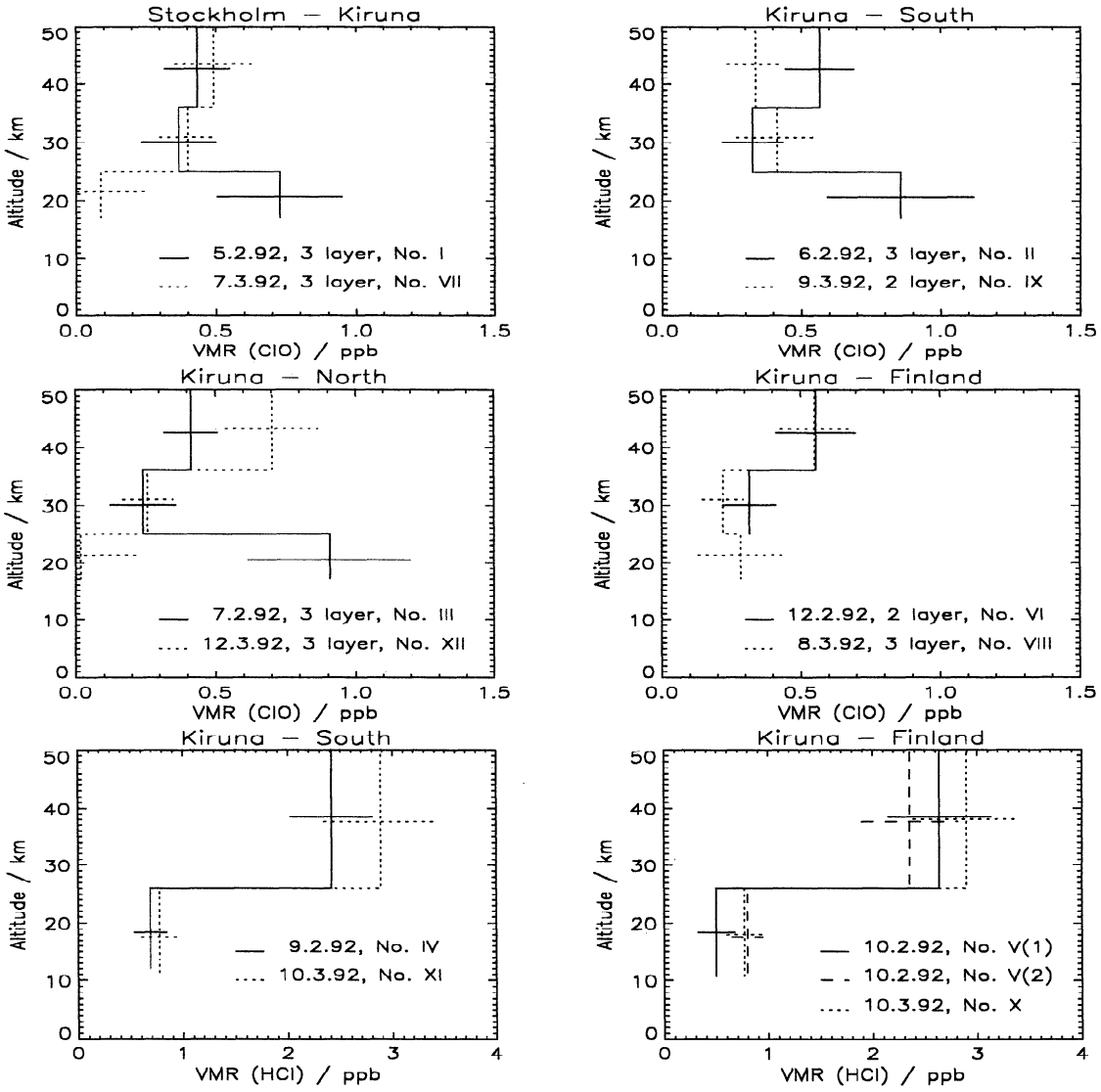

Figure 8. The Stockholm–Kiruna transfer flights and local flights of February and March 1992. The upper and middle plots are ClO profiles, the lower two plots contain HCl profiles. Solid and dashed lines are February data, dotted lines are March data.

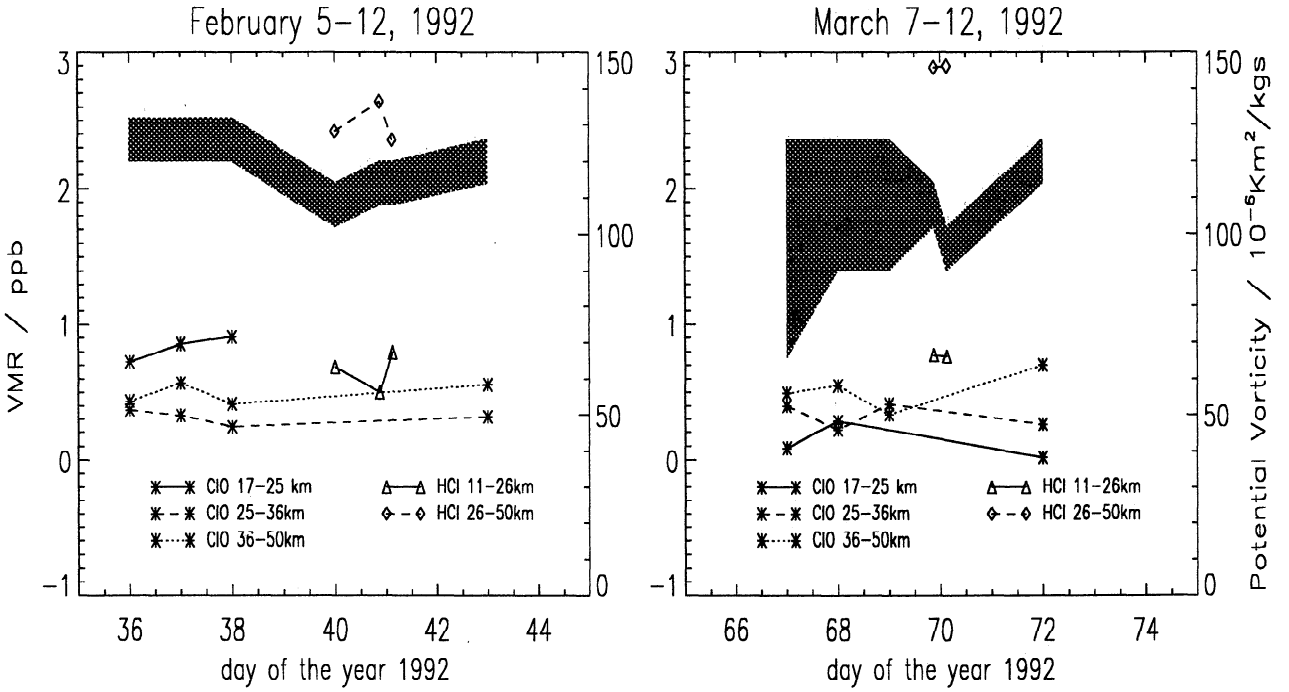

Figure 9. Temporal evolution of ClO and HCl amounts. The data are presented as a function of time for each layer together with the potential vorticity at the 550 K level at the corresponding flight route (shaded areas).

of the PV (see also Table 1). In February, all PV values along the flight routes are larger than 100 × 10^{-6} Km^2/kgs. The flight of March 7 (day 67, Stockholm-Kiruna) was across the vortex border, and the flights of March 8 and 9 (days 68 and 69) were performed close to the vortex border; therefore the PV value range is larger for these days. The two HCl measurement flights of March 10 (day 70) were from different locations with different PV values; see Figure 7 and Table 1.

The ClO profiles show high ClO concentration in the 17–25 km layer in February and a significant decrease in March. The 25–36 km layer data are approximately constant. In the upper layer (36–50 km) some variability is observed in the March data but a constant value was found for February. Differences between February and March are not significant in this layer.

HCl has been inverted with only two layers. Even though the HCl line is much stronger than the ClO line, the signal-to-noise ratio is worse because the noise of the HCl receiver is higher (see section on instrumental design) and the total integration time of the spectra is much smaller than in the case of ClO measurements because the instrument has been switched during one flight to O_3 observations at times. Above 26 km, a small increase of HCl is observed in March. Below 26 km no significant increase is observed within the error range. The flight Kiruna–Finland of February 10 (flight V) is subdivided into two parts, V(1) and V(2), separated by an ozone measurement phase. The two HCl measurements corresponding to V(1) and V(2) (Figure 8) show variations in the lower layer of the same magnitude as the deviations to the March data. The correlations of the layer errors of the HCl profiles are small, except for flight V(1) with a correlation coefficient of -0.45.

The comparison of HCl and ClO profiles shows a strong decrease of ClO in the lower stratosphere from February to March but no corresponding increase of HCl. A conversion from ClO to HCl within the observation period over northern Scandinavia can not be confirmed by our measurements.

The major reservoir species of stratospheric chlorine are HCl and $ClONO_2$. They are produced primarily by reactions with methane and NO_2, respectively:

$$Cl + CH_4 \rightarrow HCl + CH_3 \quad (12)$$

$$ClO + NO_2 \rightarrow ClONO_2 \quad (13)$$

NO_2 is produced by photochemical decomposition of HNO_3 [*Salawitch et al.*, 1993]. The dominant process between the observed periods of February and March of converting active chlorine into an inactive form seems to be reaction (13), as no increase in the observed HCl is found. This is also found in the description of chlorine chemistry by *Müller et al.* [1994], who states that the preferred production of $ClONO_2$ after the disappearing of the last polar stratospheric clouds is caused by the relative effectiveness α of reaction (12) and (13) for the removal of active chlorine, which is

$$\alpha = \frac{d[HCl]/dt}{d[ClONO_2]/dt} \approx 10^{-2} \quad (14)$$

This is consistent with Michelson interferometer for passive atmospheric sounding, balloon-borne version

(MIPAS-B) observations performed at Kiruna in the same period. Balloon measurements show that in early March most ClO_y ($HCl+ClONO_2+HOCl+ClO_x$) is in the form of $ClONO_2$ [*Oelhaf et al.*, 1994]. January data are compared with March data, and an "unexpectedly high $ClONO_2$ amount" is found in March. A similar effect has been observed by in situ measurements on board the NASA ER-2 high-altitude aircraft during the American AASE II campaign in winter 1991/1992 [*Toohey et al.*, 1993]. *Webster et al.* [1993] characterizes February and March 1992 by loss of ClO, increasing $ClONO_2$, and low HCl amounts, indicating slow HCl recovery by reaction (12). *Adrian et al.* [1994] found with ground-based Fourier transform infrared (FTIR) measurements over Kiruna in mid-March that the HCl column amount had not recovered up to that time. He states that nearly all active chlorine was converted to $ClONO_2$ instead of HCl. These results are also reproduced by model calculations with gas phase chemistry or background aerosol by *Lutman et al.* [1994b]. Infrared measurements of vertical columns made near Åre (north Sweden), reported by *Bell et al.* [1994], show a slight increase in the HCl column amount from the end of January to the middle of March.

Summary

The SUMAS has proven to be a very powerful tool in the investigation of middle atmospheric chemistry, in particular, for the observation of chlorine compounds. Error analysis shows the criticality of different error sources. In particular, large errors due to uncertainties in the pressure broadening coefficients need to be mentioned.

During the EASOE campaign, SUMAS observed a significant decrease of ClO in the lower stratosphere from February to March. The increase of HCl over the same period is not significant; therefore the assumption is supported that in this atmospheric situation the conversion to chlorine nitrate is the preferred reaction to convert active chlorine back into reservoir species.

Acknowledgments. The flight campaigns have been supported by grants from the European Union (EU). The development of the sensor was made possible by grants from the state of Bremen, the European Space Agency (ESA), and the German Ministry of Science and Technology (BMFT). We would like to thank the German Air and Space Research Organization (DLR) for excellent flight support during the campaigns.

References

Adrian, G.P., et al., First results of ground-based FTIR measurements of atmospheric trace gases in north Sweden and Greenland during EASOE, *Geophys. Res. Lett., 21*, (13), 1343–1346, 1994.

Anderson, J.G., W.H. Brune, and M.H. Profitt, Kinetics of O_3 destruction by ClO and BrO within the Antarctic vortex: An analysis based on in situ ER-2 data, *J. Geophys. Res., 94*, (11), 11,480–11,520, 1989.

Bell, W., N.A. Martin, T.D. Gardiner, N.R. Swann, and P.T. Woods, Column measurements of stratospheric trace species over Åre, Sweden in the winter of 1991-1992, *Geophys. Res. Lett., 21*, (13), 1347–1350, 1994.

Ben-Israel, A., Generalized inverses: Theory and applications, John Wiley, New York, 1974.

Braathen, G.O., F. Stordal, T. Gunstrøm, B. Knudsen, and K. Kloster, EASOE meteorology report, January–April 1992, Norw. Inst. for Air Res., Lillestrøm , 1992.

Crewell, S., Submillimeter-Radiometrie mit einem flugzeuggetragenen Empfänger zur Messung atmosphärischer Spurenstoffe, Verlag Shaker, Aachen, Germany, 1993.

Crewell, S., K. Künzi, H. Nett, T. Wehr, and P. Hartogh, Aircraft measurements of ClO and HCl during EASOE 1991/92, *Geophys. Res. Lett., 21*, (13), 1267–1270, 1994.

De Zafra, R.L., M. Jaramillo, J. Barrett, L.K. Emmons, P.M. Solomon, and A. Parrish, New observations of a large concentration of ClO in the springtime lower stratosphere over Antarctica and its implications for ozone-depleting chemistry, *J. Geophys. Res., 94*, (D9), 11,423–11,428, 1989

Farman, J.C., A. O'Neill, and R. Swinbank, The dynamics of the Arctic polar vortex during the EASOE campaign, *Geophys. Res. Lett., 21*, (13), 1195–1198, 1994

Lutman, E.R., J.A. Pyle, R.L. Jones, D.J. Lary, A.R. MacKenzie, and I. Kilbane-Dawe, Trajectory model studies of ClO_x activation during the 1991/92 northern hemispheric winter, *Geophys. Res. Lett., 21*, (13), 1419–1422, 1994a.

Lutman, E.R., R. Toumi, R.L. Jones, D.J. Lary, and J.A. Pyle, Box model studies of ClO_x deactivation and ozone loss during the 1991/92 northern hemisphere winter, *Geophys. Res. Lett., 21*,(13), 1415–1418, 1994b.

Müller, R., Th. Peter, P.J. Crutzen, H. Oelhaf, G.P. Adrian, Th. v. Clarmann, A. Wegner, U. Schmidt, and D. Lary, Chlorine chemistry and the potential for ozone depletion in the Arctic stratosphere in the winter of 1991/92, *Geophys. Res. Lett., 21*, (13), 1427–1430, 1994.

Nett, H., S. Crewell, U. Klein, J. Langen, Submillimeter-wave radiometry, European Polar Ozone Workshop, Schliersee, Germany, October 1990, *Air Pollut. Res. Rep. 34, Proceedings of the first european workshop on polar stratospheric ozone research*, pp. 81–84, Commission of the European Communities, Belgium, 1990.

Nett, H., S. Crewell, and K. Künzi, Heterodyne detection of stratospheric trace gases at submillimeter-wave frequencies, Int. Geoscience and Remote Sensing Symposium, Helsinki, Finland, 3–6 June 1991, *IEEE Cat. 91CH2971-0, vol. I*, pp. 201–204, Inst. of Electr. and Electron. Eng., New York, 1991a.

Nett, H., S. Crewell, and K. Künzi, Heterodyne receiver for airborne operation, 16th Int. Conf. Infrared and Millimeter Wave Symp., Dig., *1576*, pp. 460–461, 1991b.

Oelhaf, H., T.v. Clarmann, H. Fischer, F. Friedl-Vallon, Ch. Fritzsche, A. Linden, Ch. Piesch, M. Seefeldner, and W. Völker, Stratospheric $ClONO_2$ and HNO_3 profiles inside the arctic vortex from MIPAS-B limb emission spectra obtained during EASOE, *Geophys. Res. Lett., 21*, (13), 1263–1266, 1994.

Oh, J.J., and E.A. Cohen, Pressure broadening of ClO by N_2 and O_2 near 204 and 649 GHz and new frequency measurements between 632 And 725 GHz, *J. Quant. Spectrosc. Radiat. Transfer, 52*, 151–156, 1994.

Pickett, H.M., R.L. Poynter, and E.A. Cohen, Submillimeter, millimeter and microwave spectral line catalog, *Applied Optics, 24*, 2235–2240, 1985, Revision 3, Tech. Rep. 80–23, Jet Propulsion Laboratory, 1991.

Rodgers, C.D, Retrieval of atmospheric temperature and composition from remote measurements of thermal radiation, *Rev. Geophys., 14*, (4), 609–624, 1976.

Rodgers, C.D., Characterization and error analysis of profiles retrieved from remote sounding measurements, *J. Geophys. Res., 95*, (D5), 5587–5595, 1990.

Salawitch, R.J., et al., Chemical loss of ozone in the arctic polar vortex in the winter of 1991–1992, *Science, 261*, 1146–1149, 1993.

Solomon, P., B. Connor, R. deZafra, A. Parrish, J. Barret, and M. Jaramillo, Observations of abnormally high concentrations of chlorine monoxide at low altitudes in the antarctic spring stratosphere, *Nature, 328*, 411-413, 1987.

Solomon, S., Progress towards a quantitative understanding of Antarctic ozone depletion, *Nature, 347*, 347–353, 1990.

Stachnik, R.A., J.C. Hardy, J.A. Tarsala, and J.W. Waters, Submillimeterwave heterodyne measurements of stratospheric ClO, HCl, O_3, and HO_2: First results, *Geophys. Res. Lett., 19*, (19), 1931–1934, 1992.

Toohey, D.W., L.M. Avallone, L.R. Lait, P.A. Newman, M.R. Schoeberl, D.W. Fahey, E.L. Woodbridge, and J.G. Anderson, The seasonal evolution of reactive chlorine in the northern hemisphere stratosphere, *Science, 261*, 1134–1135, 1993.

Waters, J.W., Absorption and emission by atmospheric gases, *Methods Exp. Phys.,Part B, 12*, 142–176, 1976.

Waters, J.W., L. Froidevaux, W.G. Read, G.L. Manney, L.S. Elson, D.A. Flower, R.F. Jarnot, and R.S. Harwood, Stratospheric ClO and ozone from the microwave limb sounder on the upper atmosphere research satellite, *Nature, 362*, 597–602, 1993.

Webster, C.R., R.D. May, D.W. Toohey, L.M. Avallone, J.G. Anderson, P. Newman, L. Lait, M.R. Schoeberl, J.W. Elkins, and K.R. Chan, Chlorine chemistry on polar stratospheric cloud particles in the arctic winter, *Science, 261*, 1130–1133, 1993.

Wehr, T., Bestimmung atmosphärischer Spurengasgehalte aus Spektren eines flugzeuggestützten Submillimeter-Radiometers, Diploma thesis, Inst. of Remote Sens., University of Bremen, Bremen, Germany, 1993

World Meteorological Organization, Atmospheric ozone 1985, WMO global ozone research and monitoring project report no. 16, Tech. Rep., Geneva, Switzerland, 1985.

S. Crewell, Physics Department, State University of New York (SUNY), NY 11794-3800, (e-mail: screwell@gelua1.uars.sunysb.edu)

K. Künzi, J. Urban, and T. Wehr, University of Bremen, Institute of Environmental Physics, P.O. Box 330440, 28334 Bremen, Germany, (e-mail: kunzi@physik.uni-bremen.de; jo@atm.physik.uni-bremen.de; wehr@physik.uni-bremen.de)

H. Nett, ESA/ESTEC, ENVISAT Programme Department (NWP), P.O. Box 299, NL-2200 AG Noordwijk, Netherlands, (e-mail: hnett@jw.estec.esa.nl)

J. Langen, ESA/ESTEC VRA, P.O. Box 299, NL-2200 AG Noordwijk, Netherlands, (e-mail: jlangen@estec.esa.nl)

(Received September 16, 1994; revised June 11, 1995; accepted June 16, 1995.)